

Inverted V-shaped evolution of superconducting temperature in SrBC under pressure

Ru-Yi Zhao(赵如意), Xun-Wang Yan(闫循旺), and Miao Gao(高淼)
Citation: Chin. Phys. B, 2021, 30 (**7**): 076301. DOI: 10.1088/1674-1056/abfbcc
Journal homepage: http://cpb.iphy.ac.cn; http://iopscience.iop.org/cpb

What follows is a list of articles you may be interested in

Two-dimensional MnN utilized as high-capacity anode for Li-ion batteries

Junping Hu(胡军平), Zhangyin Wang(王章寅), Genrui Zhang(张根瑞), Yu Liu(刘宇), Ning Liu(刘宁), Wei Li(李未), Jianwen Li(李健文), Chuying Ouyang(欧阳楚英), and Shengyuan A. Yang(杨声远)
Chin. Phys. B, 2021, 30 (**4**): 046302. DOI: 10.1088/1674-1056/abdda8

Effect of strain on electrochemical performance of Janus MoSSe monolayer anode material for Li-ion batteries: First-principles study

Guoqing Wang(王国庆), Wenjing Qin(秦文静), and Jing Shi(石晶)
Chin. Phys. B, 2021, 30 (**4**): 046301. DOI: 10.1088/1674-1056/abca24

Theoretical analysis of cross-plane lattice thermal conduction in graphite

Yun-Feng Gu(顾云风)
Chin. Phys. B, 2019, 28 (**6**): 066301. DOI: 10.1088/1674-1056/28/6/066301

Unconventional lattice dynamics in few-layer h-BN and indium iodide crystals

Gan Hu(胡干), Jian-Qi Huang(黄建啟), Ya-Ning Wang(王雅宁), Teng Yang(杨腾), Bao-Juan Dong(董宝娟), Ji-Zhang Wang(王吉章), Bo Zhao(赵波), Sajjad Ali(阿里·萨贾德), Zhi-Dong Zhang(张志东)
Chin. Phys. B, 2018, 27 (**8**): 086301. DOI: 10.1088/1674-1056/27/8/086301

Superconductivity in electron-doped arsenene

Xin Kong(孔鑫), Miao Gao(高淼), Xun-Wang Yan(闫循旺), Zhong-Yi Lu(卢仲毅), Tao Xiang(向涛)
Chin. Phys. B, 2018, 27 (**4**): 046301. DOI: 10.1088/1674-1056/27/4/046301

Inverted V-shaped evolution of superconducting temperature in SrBC under pressure*

Ru-Yi Zhao(赵如意)[1], Xun-Wang Yan(闫循旺)[2], and Miao Gao(高淼)[1,†]

[1] Department of Physics, School of Physical Science and Technology, Ningbo University, Ningbo 315211, China
[2] College of Physics and Engineering, Qufu Normal University, Qufu 273165, China

(Received 19 March 2021; revised manuscript received 23 April 2021; accepted manuscript online 27 April 2021)

Based on density functional first-principles calculations and anisotropic Eliashberg equations, we have investigated the electronic structure, lattice dynamics, and phonon-mediated superconductivity in newly synthesized layered compound SrBC under pressure. Different from LiBC and MgB_2, our calculations surprisingly reveal that SrBC is isotropic in compressibility, due to the accumulation of substantial electrons in the interstitial region. We find that the Sr phonons strongly couple with B-$2p_z$ orbital and the interstitial states, giving rise to a two-gap superconductivity in SrBC, whose transition temperature shows an inverted V-shaped dependence on pressure. The maximal transition temperature is about 22 K at 50 GPa. On both sides of 50 GPa, the transition temperature exhibits quasi-linear variation with positive and negative slopes, respectively. Such a variation of transition temperature is infrequent among phonon-mediated superconductors. The competition between enhanced electron–phonon matrix element and hardened phonons plays an essential role in governing the behavior of the critical temperature.

Keywords: SrBC, phonon-mediated superconductivity, anisotropic Eliashberg theory, first-principles calculation, maximally localized Wannier functions

PACS: 63.20.D−, 63.20.kd, 74.20.Pq, 74.70.Dd **DOI:** 10.1088/1674-1056/abfbcc

1. Introduction

The outstanding superconductivity of MgB_2 stems from its unique electronic structure, whereas both the σ-bonding bands and π-bonding band cross the Fermi level simultaneously.[1–3] The underlying superconducting mechanism in MgB_2 has been well understood by the strong-coupling anisotropic Migdal–Eliashberg theory. The consensus is that MgB_2 is a two-gap phonon-mediated superconductor.[4,5] Finding MgB_2-type superconductor has drawn lots of attention both theoretically and experimentally. A fascinating analogue is hole-doped LiBC, namely, Li_xBC. By introducing Li vacancies, the σ bands were predicted to be partially filled, leading to a high T_c about 100 K.[6] However, the Li vacancies cause significant lattice distortion, which impedes the metallization of the σ bands.[7] As a result, no superconducting transition was observed in Li_xBC.[8–11] To avoid the formation of Li vacancies, introducing excess boron was proposed to be an alternative way to realize hole doping of LiBC, for example, Li_2B_3C, $Li_3B_4C_2$,[12] and $Li_4B_5C_3$.[13] We further systematically studied the electron–phonon coupling (EPC) in free-standing and strained trilayer film LiB_2C_2.[14] It was found that the highest T_c can be achieved is 125 K for LiB_2C_2 film under biaxial tensile strain of 8%.

In addition to doping holes, Haque *et al*. suggested that doping electrons into LiBC by replacing Li with alkaline-earth metal M (M = Mg, Ca, Sr, or Ba) may induce superconducting states.[15] For example, the T_c was estimated to be 51 K for MgBC with McMillan–Allen–Dynes formula.[15] It was shown by first-principles calculation that MBC has two energy bands crossing the Fermi level, similar to the case in MgB_2. Hence, it is necessary to determine the T_c through self-consistently solving the anisotropic Eliashberg equations, rather than using the semi-empirical McMillan–Allen–Dynes formula. Very recently, utilizing the CALYPSO structure prediction method, SrBC was found to be stable at 50 GPa.[16] In particular, SrBC has been successfully synthesized in experiment.[16] It is thus quite interesting to accurately investigate the phonon-mediated superconductivity in SrBC and its evolution under pressure. Especially, whether the two metallic bands of SrBC can give rise to the high-T_c two-gap superconductivity as in MgB_2.

In this work, the electronic structure, lattice dynamics, EPC, and superconductivity in SrBC are studied from ambient pressure to 100 GPa by means of the first-principles calculations. The lattice constants of SrBC show excellent isotropy during compression. This most likely originates from the appearance of interstitial electronic states between two boron-carbon sheets. B-$2p_z$ orbital and the interstitial states contribute mostly to the density of states around the Fermi level. We find that Sr phonons possess strong coupling with B-$2p_z$ orbital and interstitial states. Through Wannier interpolation

*Project supported by the National Natural Science Foundation of China (Grant Nos. 11974194 and 11974207) and K. C. Wong Magna Fund in Ningbo University.

†Corresponding author. E-mail: gaomiao@nbu.edu.cn

© 2021 Chinese Physical Society and IOP Publishing Ltd

technique, the EPC constant λ is accurately calculated to be 0.709 at ambient pressure. Interestingly, there is a dome-like feature for λ with the increase of the applied pressure. This can be explained by the competition between enhanced electron–phonon matrix element and hardened phonons. By solving the anisotropic Eliashberg equations, SrBC is determined to be a two-gap superconductor. The T_c shows an inverted V-shaped relationship with pressure. SrBC can achieve its maximal T_c of 22 K under 50 GPa. Below 50 GPa, T_c almost increases linearly, with a positive rate of 0.18 K/GPa. Contrarily, a negative slope of -0.08 K/GPa is found beyond 50 GPa. The slightly different pressure dependence for λ and T_c is due to the enlarged energy scale of electron pairing, as indicated by the characteristic phonon frequency.

2. Methods

In our calculations, the first-principles package, Quantum-ESPRESSO, was adopted.[17] We calculated the electronic states and phonon perturbation potentials[18] using the generalized gradient approximation (GGA) of Perdew–Burke–Ernzerhoff formula[19] and the optimized norm-conserving Vanderbilt pseudopotentials.[20] After convergence test, the kinetic energy cut-off and the charge density cut-off were chosen to be 80 Ry and 320 Ry, respectively. The charge densities were calculated on a $\boldsymbol{k}$ mesh of $24\times24\times12$ points in combination with a Methfessel–Paxton smearing[21] of 0.02 Ry. The dynamical matrices and the perturbation potentials were computed on a $8\times8\times4$ mesh, based on the density-functional perturbation theory.[22] Ten randomly-centered s-type Gaussian functions were used as the initial guess to construct the maximally localized Wannier functions (MLWFs).[23] When checking the convergence of EPC constant λ, the phonon grid was fixed to $24\times24\times12$ points, the electron grid was extended from $24\times24\times12$, to $36\times36\times18$, to $48\times48\times24$, and finally to $72\times72\times36$ points.[24] The Dirac δ-functions for electrons and phonons were smeared out by a Gaussian function with the widths of 80 meV and 0.5 meV, respectively. An electron grid of $48\times48\times24$ points was employed in solving the anisotropic Eliashberg equations.[24–26] The number of Matsubara frequency grid points was chosen to be 300. The highest temperature with non-zero superconducting gap corresponds to the transition temperature. In practice, the threshold value for nonvanishing gap was set to 0.01 meV during the numerical iterations.

3. Results and discussion

SrBC is isostructural to LiBC, in which the boron-carbon sheet forms a honeycomb lattice, while Sr atoms occupy the hollow sites between two adjacent boron-carbon sheets. At ambient pressure, the lattice constants are optimized as $a=3.0122$ Å and $c=8.9909$ Å, in excellent agreement with previous results.[15,16] The band structure of SrBC is shown in Fig. 1(a). Unlike semiconducting LiBC, SrBC is a metal, in which two bands crossing the Fermi level. Particularly, the energy gap that found in LiBC is absent near the Fermi level. Thus, the electronic structure of SrBC can not be simply regraded as the rigid shift of Fermi level of LiBC. There is strong hybridization among the $2p_x$ and $2p_y$ orbitals of boron and carbon atoms, as revealed by the peak of the orbital-resolved density of states (DOS) around -3.5 eV [Fig. 1(b)]. The hybridization that occurs in the two-dimensional honeycomb sheet will generate bonding σ and antibonding σ^* bands. The maximum of the σ bands is about -1.4 eV, corresponding to the dispersionless bands along Γ–A line. While, the energy of the σ^* bands is well above the Fermi level. As a consequence, the contribution to $N(0)$ (DOS at the Fermi level) from $2p_x$ and $2p_y$ orbitals of boron and carbon atoms is tiny. The overlapping between the $2p_z$ orbitals of carbon and boron atoms will engender π and π^* bands. As we see, there is a pseudo gap for p_z-related DOS, roughly around -1.5 eV [Fig. 1(b)]. These bands can be respectively assigned to π and π^* bands below and above the pseudo gap. Therefore, the π^* bands (mainly from the B-$2p_z$ orbital) make a large contribution to $N(0)$. Moreover, Sr-5s orbital occupies nonnegligible proportion of $N(0)$. These observations are different from the conclusion drawn in Ref. [15], in which the partially filled energy bands were assigned to σ and π bands, respectively.

Detailed analysis shows that the summation of orbital-resolved DOS does not match the total DOS near the Fermi level [Fig. 1(c)]. Specifically, the orbital-resolved DOS is just about 58.8% of the total DOS. This indicates that there exist copious interstitial states. As confirmed by the integrated local DOS, abundant charge accumulation can be clearly observed in the middle region of two neighboring boron-carbon sheets [Fig. 1(g)]. We further project the weights of B-$2p_z$, C-$2p_z$, Sr-5s, and interstitial states onto the Fermi surfaces [Figs. 1(h)–1(k)]. The two incompletely filled energy bands yield two Fermi surfaces. The Fermi-surface states close to the K point mainly comprise of the B-$2p_z$ orbital [see the bottom panel of Fig. 1(h)]. Sr-5s orbital contributes mostly to the Fermi pocket surrounding the Γ point. The interstitial states dominate the contribution to the hexagonal cylinder-like Fermi surface and states near the M point. We also map the $\boldsymbol{k}$-resolved EPC constant, i.e., $\lambda_{\boldsymbol{k}n}$ on the Fermi surfaces. Obviously, the interstitial states on the hexagonal cylinder-like Fermi surface strongly couple with phonons [Fig. 1(l)].

Under 50 GPa, the lattice constants of SrBC are calculated to be $a=2.7900$ Å and $c=8.3331$ Å. Interestingly, a and c shrink about 7.38% and 7.32%, respectively, compared with the data obtained at ambient pressure. This means that SrBC is almost isotropic in compressibility. The isotropy of compress-

ibility can at least retain to 100 GPa, under which the lattice constants are compressed by 11.2% and 11.1% along a and c axes, respectively. It is known that layered compounds always exhibit large anisotropy in compressibility, which reflects the bonding nature along different directions in the material. For instance, the compressibility along the c axis is five times that along the a axis for LiBC.[27] Similar situation was also reported in MgB_2, where the lattice constant c decreases faster with pressure than a.[28] The greater stiffness along the c axis of SrBC compared to LiBC is closely related to the presence of interstitial states between boron-carbon sheets. After applying pressure, the band becomes more dispersive [Fig. 1(d)]. Consequently, the sharp peaks in DOS are broadened [Fig. 1(e)]. There still exist substantial interstitial states, which contribute 38.0% of $N(0)$ [Fig. 1(f)]. Due to the enlarged band widths, the Fermi pocket around the Γ point disappears. The weights of B-2p_z, C-2p_z, Sr-5s, and interstitial states on the Fermi surfaces behavior similarly to the case under ambient pressure [Figs. 1(m)–1(p)]. Remarkably, the EPC is enhanced significantly [Fig. 1(q)].

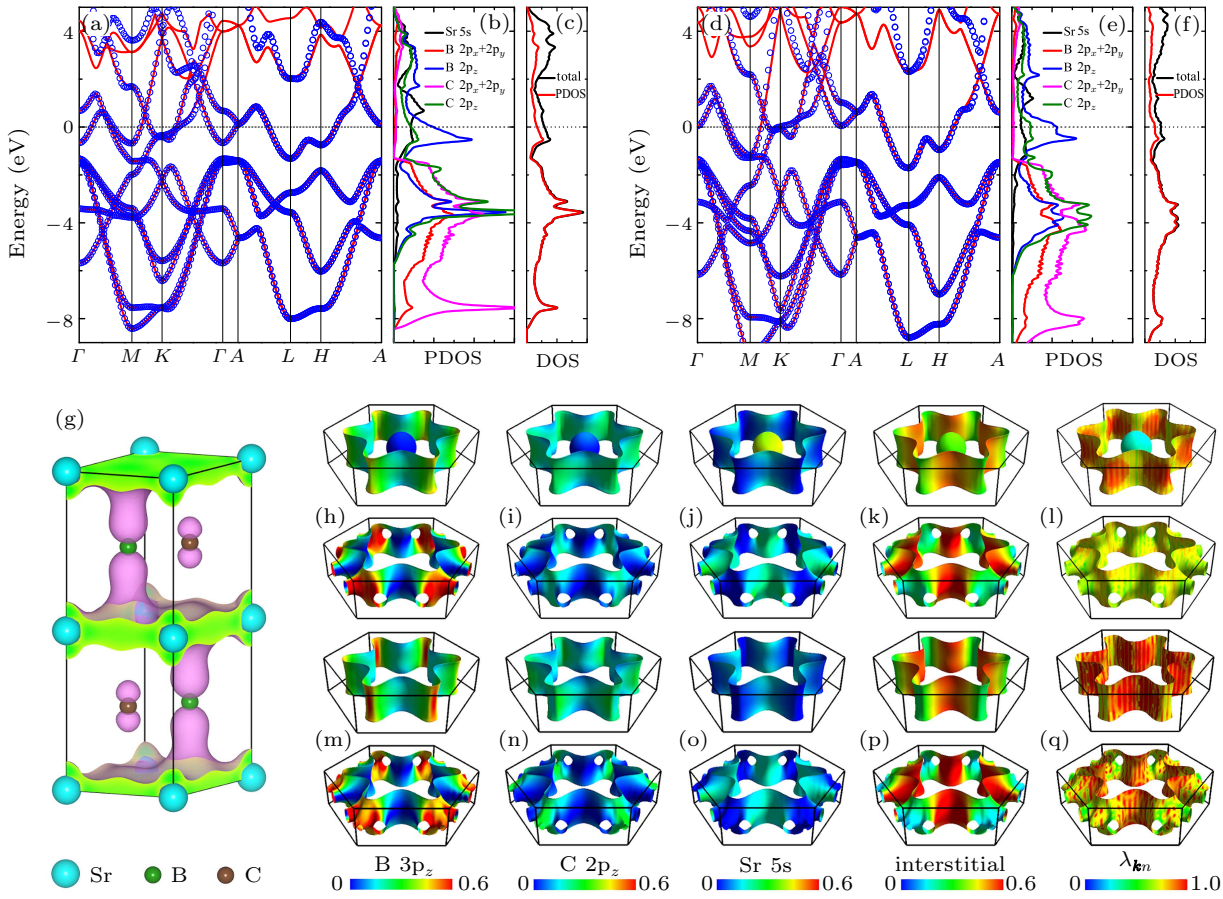


Fig. 1. Electronic structure for SrBC. (a) Band structure under ambient pressure. The red lines and blue circles denote the bands obtained by first-principles calculation and interpolating the real-space Hamiltonian, respectively. The Fermi level is set to zero. (b) Orbital-resolved DOS. (c) Total DOS. (d) Band structure under 50 GPa. (e) Orbital resolved and (f) total DOS under 50 GPa. (g) Isosurface of integrated local density of states from −0.1 eV to 0.1 eV under ambient pressure. The isovalue is selected as 1.0×10^{-3} e/Bohr^3. (h)–(q) The weights of B 2p_z, C 2p_z, Sr 5s, interstitial states, and momentum-resolved EPC constants on the Fermi surfaces. Here (h)–(l) correspond to the results under ambient pressure, (m)–(q) stand for the datum of 50 GPa.

Figure 2 shows the lattice dynamics of SrBC. Although, SrBC was proved to be stable above 50 GPa, there is no imaginary phonon frequency under ambient pressure [Fig. 2(a)]. A small frequency gap at about 25 meV is found. Below the gap, there are six branches of phonons, which can be assigned to the vibration of Sr, due to its greater atomic mass than those of boron and carbon. This is confirmed by the projected phonon DOS $F(\omega)$ [Fig. 2(b)]. As reflected by λ_{qv}, Sr-associated phonons have strong coupling with electrons, especially the interstitial states. Under 50 GPa, the phonons show markedly hardening [Fig. 2(c)], owing to the enhanced interatomic force constants. For example, the highest frequency is amplified by 36.5% with respect to the ambient pressure. Similar to the electronic DOS, the peaks of projected $F(\omega)$ are evidently reduced [Fig. 2(d)]. The number of Sr-associated phonon modes with sizeable λ_{qv} increases. This will lead to enlarged EPC constant, self-consistent with Fig. 1(q).

The Eliashberg spectral function $\alpha^2F(\omega)$, total $F(\omega)$, and accumulated $\lambda(\omega)$ are shown in Fig. 3. At ambient pressure, $\alpha^2F(\omega)$ displays multi-peak characteristics [Fig. 3(a)]. Two peaks locate below the frequency gap. By integrating $\alpha^2F(\omega)$, the EPC constant λ is accurately determined to be 0.709. Under 50 GPa, all these peaks of $\alpha^2F(\omega)$ are blue-shifted, combined with obvious broadening [Fig. 3(b)]. Sup-

pose that the phonon linewidth is unaffected by pressure, then $\lambda_{qv} \propto \omega_{qv}^{-2}$, thus the hardened phonons will cause abatement of EPC. Surprisingly, the heights of the low-frequency peaks abnormally increase. As a result, the EPC constant λ is boosted to 0.783, slightly larger than that in MgB_2 acquired by Wannier interpolation technique.[26,29,30] The low-frequency two peaks dominate the EPC process, since Sr-related phonons already take 80.7% and 86.1% of the total λ under ambient pressure and 50 GPa, respectively, as marked by the black arrows (Fig. 3).

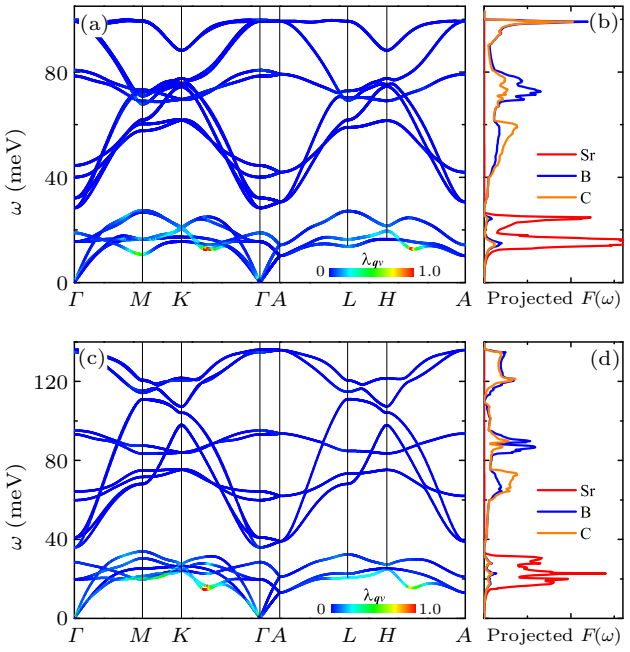


Fig. 2. Lattice dynamics of SrBC. (a) Phonon spectrum with a color representation of λ_{qv} and (b) projected phonon DOS generated by quasi-harmonic approximation, under ambient pressure. (c) Phonon spectrum and (d) projected phonon DOS under 50 GPa.

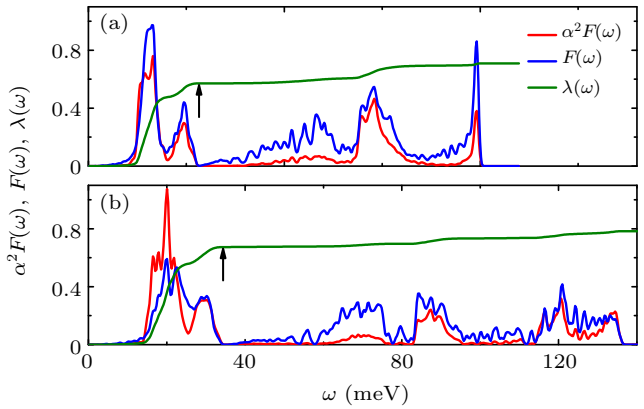


Fig. 3. The Eliashberg spectral function $\alpha^2F(\omega)$, total $F(\omega)$, and accumulated $\lambda(\omega)$ under ambient pressure (a) and 50 GPa (b). Here $\lambda(\omega)$ is computed using the formula $2\int_0^{\omega}\frac{1}{\omega'}\alpha^2F(\omega')\mathrm{d}\omega'$. Black arrows roughly point out the highest frequencies of Sr phonons under different pressures.

To clarify the physical reason for abnormal rise of λ under 50 GPa, we calculated the Fermi surface nesting function $\xi(\boldsymbol{q})$, EPC matrix element weighted nesting function $\gamma(\boldsymbol{q})$, and $\boldsymbol{q}$-resolved EPC constant $\lambda(\boldsymbol{q})$. $\xi(\boldsymbol{q})$ and $\gamma(\boldsymbol{q})$ are computed through

$$\xi(\boldsymbol{q}) = \frac{1}{N(0)N_{\boldsymbol{k}}}\sum_{nm\boldsymbol{k}}\delta(\varepsilon_{\boldsymbol{k}}^{n})\delta(\varepsilon_{\boldsymbol{k}+\boldsymbol{q}}^{m}), \tag{1}$$

$$\gamma(\boldsymbol{q}) = \frac{1}{N(0)N_{\boldsymbol{k}}}\sum_{nm\boldsymbol{k}v}|g_{\boldsymbol{k},\boldsymbol{q}v}^{nm}|^2\delta(\varepsilon_{\boldsymbol{k}}^{n})\delta(\varepsilon_{\boldsymbol{k}+\boldsymbol{q}}^{m}), \tag{2}$$

Here $\omega_{\boldsymbol{q}v}$ corresponds the phonon frequency and $g_{\boldsymbol{k},\boldsymbol{q}v}^{nm}$ represents the EPC matrix element. (n,m) and v denote the indices of energy bands and phonon mode, respectively. $\varepsilon_{\boldsymbol{k}}^{n}$ and $\varepsilon_{\boldsymbol{k}+\boldsymbol{q}}^{m}$ are the eigenvalues of the electronic states with respect to the Fermi energy. $N_{\boldsymbol{k}}$ is the total number of $\boldsymbol{k}$ points in the fine mesh. $\lambda(\boldsymbol{q}) = \sum_v \lambda_{\boldsymbol{q}v}$, in which $\lambda_{\boldsymbol{q}v}$ reads

$$\lambda_{\boldsymbol{q}v} = \frac{2}{\hbar N(0)N_{\boldsymbol{k}}}\sum_{nm\boldsymbol{k}}\frac{1}{\omega_{\boldsymbol{q}v}}|g_{\boldsymbol{k},\boldsymbol{q}v}^{nm}|^2\delta(\varepsilon_{\boldsymbol{k}}^{n})\delta(\varepsilon_{\boldsymbol{k}+\boldsymbol{q}}^{m}). \tag{3}$$

Firstly, we can rule out the nesting function $\xi(\boldsymbol{q})$ as the main factor that causes amplified λ, since $\xi(\boldsymbol{q})$ shows overall reduction with the increase of pressure [Fig. 4(a)]. Interestingly, $\gamma(\boldsymbol{q})$ is significantly improved, especially under 50 GPa, compared with that at ambient pressure [Fig. 4(b)]. It has been demonstrated that the phonons are hardened under pressure. This is harmful to the enlargement of EPC constant λ, according to Eq. (3), whereas $\omega_{\boldsymbol{q}v}$ is the denominator. As shown in Fig. 4(c), the preponderance in $\gamma(\boldsymbol{q})$ under pressure is gradually condensed in $\lambda(\boldsymbol{q})$. However, the EPC strength of λ under 50 GPa still overwhelms that under ambient pressure. Hence, the increase of λ under 50 GPa can be attributed to the enhancement of EPC matrix elements close to the Fermi level, i.e., $\gamma(\boldsymbol{q})$. While, the maximal phonon frequency reaches 159.0 meV under 100 GPa. This means that there will be a drop in λ at higher pressure, due to the competition between increscent $\gamma(\boldsymbol{q})$ and diminished $\omega_{\boldsymbol{q}v}^{-1}$ [see Eqs. (2) and (3)]. This is just the case for 100 GPa. The detailed change rule of λ is given in Fig. 6.

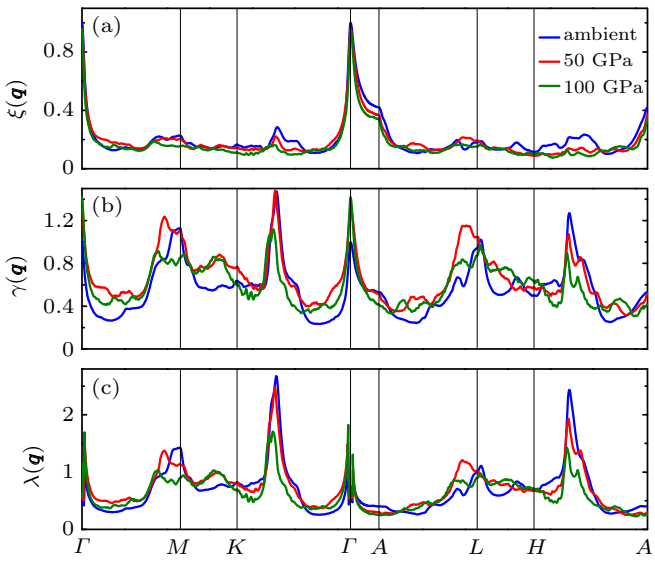


Fig. 4. Comparisons of nesting function $\xi(\boldsymbol{q})$, EPC matrix element weighted nesting function $\gamma(\boldsymbol{q})$, and $\boldsymbol{q}$-resolved EPC constant $\lambda(\boldsymbol{q})$ under different pressures.

By solving the anisotropic Eliashberg equations, we can obtain the superconducting transition temperature and the distribution of superconducting gaps on the Fermi surfaces [Fig. 5]. Here, the Coulomb pseudopotential μ^* was set to a standard value of 0.10.[31,32] SrBC is a two-gap superconductor, whose T_c is about 13 K under ambient pressure [Fig. 5(a)]. At 5 K, the average values for these two superconducting gaps are computed to be 1.98 meV and 1.14 meV, respectively. The higher superconducting gap mainly locates on the hexagonal cylinder-like Fermi surface [Fig. 5(c)]. While, the lower gap stems from the Fermi surface close to the boundaries of the Brillouin zone [Fig. 5(d)]. The distributions of $\Delta_{\boldsymbol{k}n}$ are in agreement with the weights of $\lambda_{\boldsymbol{k}n}$ [Fig. 1(l)]. Under 50 GPa, these two gaps are enlarged to 3.79 meV and 2.38 meV, respectively [Fig. 5(b)], resulting in a boosted T_c of 22 K. The distributions of $\Delta_{\boldsymbol{k}n}$ are similar to those under ambient pressure [Figs. 5(e) and 5(f)].

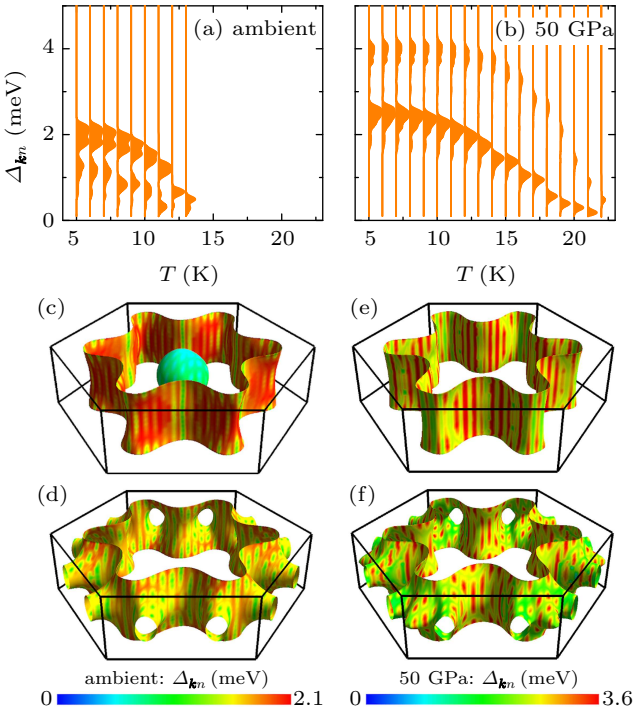


Fig. 5. Temperature dependence of gap values $\Delta_{\boldsymbol{k}n}$ on the Fermi surface for SrBC under ambient pressure (a) and 50 GPa (b). The distribution of superconducting gaps on the Fermi surfaces at 5 K for SrBC under ambient pressure (c)–(d) and 50 GPa (e)–(f).

Figure 6 presents the evolutions of EPC constant λ and T_c of SrBC under pressure. The EPC constant λ shows dome-like dependence of pressure. This is because that λ is controlled by the competition between the increscent $\gamma(\boldsymbol{q})$ and diminished $\omega_{\boldsymbol{q}\nu}^{-1}$, as analyzed above. λ reaches the maximal value at 25 GPa. An inverted V-shaped feature is observed for the superconducting T_c, which does not exactly follow the change rule of λ. In particular, the optimal pressure for T_c is about 50 GPa. Furthermore, the decay of T_c is slower than that of λ. This originates from the enhanced phonon frequencies under pressure, which decide the energy scale of superconducting pairing. As an evidence, from ambient pressure to 100 GPa, the logarithmic average frequency $\omega_{\log}$ [33] is determined as 21.44, 22.84, 25.29, 27.84, and 30.52 meV, respectively. Absorbingly, the T_c is quasi-linear with pressure below and above 50 GPa, with slopes being 0.18 K/GPa and −0.08 K/GPa, respectively. The link between T_c and $N(0)$ is quite weak. Specifically, $N(0)$ equals 0.877, 0.791, 0.799, 0.77, and 0.696 states/spin/eV/cell from ambient pressure to 100 GPa, giving rise to a monotonous reduction. The T_c determined by McMillan–Allen–Dynes (MAD) formula[33] is also given in Fig. 6. When sampling the Brillouin zone, dense grids are absolutely necessary to gain convergent EPC-related quantities. As a comparison, the MAD T_c for SrBC under ambient pressure is 8.9 K by setting the Coulomb pseudopotential μ^* to 0.1. This value was overestimated by 31.5% in Ref. [15].

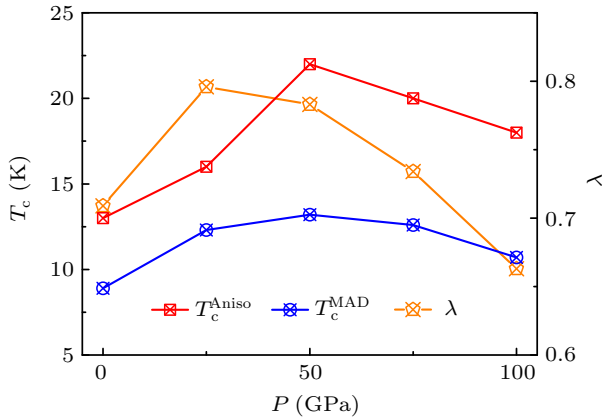


Fig. 6. Calculated superconducting transition temperatures of SrBC under different pressures. Here $T_c^{\rm Aniso}$ and $T_c^{\rm MAD}$ represent the critical temperatures determined by solving the anisotropic Eliashberg equations and the McMillan–Allen–Dynes formula, respectively. The pressure dependence of EPC constant λ is also given.

The pressure dependence of T_c for SrBC is infrequent among phonon-mediated superconductors. For MgB_2, T_c decreases quasi-linearly under low pressure with solpe dT_c/dP between −0.8 K/GPa and −2.0 K/GPa.[34–37] Under higher pressure, it was found that the T_c follows a purely quadratic drop.[34] Especially, the T_c of MgB_2 has already been reduced to 20.9 K at 19.2 GPa.[38] The physical reason for degressive T_c can by explained by a combination of hardened phonons and depressed $N(0)$, particularly the phonons.[39] In contrast, an enhancement of T_c was reported in MgB_2 due to phonon softening under tensile strain.[40] The transition temperatures of elemental superconductors, examplified by Al[41] and Pb,[42] also decrease monotonically with pressure. Ca and Y are not superconductive under ambient pressure. While, superconducting transitions in Ca and Y show positive dependence on high pressure. In particular, the transition temperatures can achieve 19.5 K[43] and 25 K,[44] under 115 GPa and 161 GPa, respectively. The superconductivity of rare-earth metals under high pressure has also been extensively studied, such as in La. Under ambient pressure, La takes either double

hexagonal-close-packed (dhcp) phase or face-centered cubic (fcc) phase, with T_c being 5 K and 6 K.[45,46] However, the behavior of T_c is more complicated under pressure, closely related to the phase transition. For example, the T_c is firstly enhanced after the occurrence of structural phase transition into a distorted fcc structure near 5.4 GPa. Notable oscillation in T_c can be observed for the distorted fcc phase, with the highest T_c being about 13 K.[47,48] Further increasing the pressure, La undergos distorted fcc to fcc, and fcc to another distorted fcc phase transitions. The transition temperature basically shows monotone decline above 50 GPa, and finally goes down to 2.2 K at 140 GPa.[49]

For MgB_2, it was suggested that the enlargement of lattice constant along the c axis can increase $N(0)$ and shift the σ band upward.[50] Correspondingly, the hole number in the σ band increases and a higher T_c can be expected. Moreover, reducing the lattice constant along a axis has similar effect with enlarging the c axis. Since SrBC achieves its highest T_c under 50 GPa. Followed the prediction in MgB_2, we further examine the possibility to enhance the T_c by respectively modulating the lattice constants along different directions. For simplicity, the lattice constants of SrBC under 50 GPa are labelled as a_0 and c_0. Specifically, we systematically investigate the phonon-mediated superconductivity under four situations, i.e., $c = 1.15c_0$, $c = 0.90c_0$, $a = 1.15a_0$, and $a = 0.85a_0$. When adjusting the lattice constant along the c axis, the a-axis cell parameter is unchanged, and vice versa. Similar to the case of MgB_2, we find that the maximum of σ bands increases by 0.47 meV and 0.61 meV for $c = 1.15c_0$ and $a = 0.85a_0$, respectively. While, it decreases by 0.45 meV and 0.43 meV for $c = 0.90c_0$ and $a = 1.15a_0$. The σ bands are still completely filled for all these cases. In particular, we find that the dependence of T_c in SrBC on the lattice constants is more complicated than that in MgB_2. Interestingly, only $c = 0.90c_0$ can boost the T_c to a higher value of 31 K among the studied four situations. According to our calculations, we find that $N(0) = 0.961$ states/spin/eV/cell, $\lambda = 1.052$, and $\omega_{log} = 25.66$ meV for $c = 0.90c_0$. The enhanced T_c is probably related to the aggrandizement of $N(0)$.

4. Conclusion

In summary, we have presented the first-principles results of electronic structure, lattice dynamics, EPC, and phonon-mediated superconductivity for layered SrBC. Although, SrBC is isostructural to LiBC, significant differences are unmasked by our calculations. For instance, SrBC is inherently metallic with two partially filled energy bands, in comparison with the insulating nature of LiBC. The electronic states around the Fermi level mainly consist of B-$2p_z$ orbital and considerable interstitial states. Moreover, SrBC is isotropic in compression, contrast sharply to LiBC. Based on these observations, SrBC can not be concluded as an electron-doped LiBC-like compound with rigid Fermi-level shifting. The EPC strength λ is accurately determined to be 0.709 under atmospheric pressure. Based on anisotropic Eliashberg theory and Wannier interpolation, we find that SrBC is a two-gap superconductor with T_c of 13 K, which is evidently smaller with respect to MgB_2. This is because that low-frequency Sr phonons govern the EPC process of SrBC rather than high-frequency bond-stretching boron-related phonon modes as in MgB_2. Since SrBC is stable above 50 GPa, we have systematically examined the evolution of superconductivity under pressure. In particular, an inverted V-shaped evolution of T_c is revealed, with the highest T_c being 22 K at 50 GPa. This phenomenon is scarce among phonon-mediated superconductors, and stems from the balance between enhanced EPC matrix element and hardened phonons.

References

[1] An J M and Pickett W E 2001 *Phys. Rev. Lett.* **86** 4366
[2] Kong Y, Dolgov O V, Jepsen O and Andersen O K 2001 *Phys. Rev. B* **64** 020501
[3] Kortus J, Mazin I I, Belashchenko K D, Antropov V P and Boyer L L 2001 *Phys. Rev. Lett.* **86** 4656
[4] Choi H J, Roundy D, Sun H, Cohen M L and Louie S G 2002 *Phys. Rev. B* **66** 020513
[5] Choi H J, Roundy D, Sun H, Cohen M L and Louie S G 2002 *Nature* **418** 758
[6] Rosner H, Kitaigorodsky A and Pickett W E 2002 *Phys. Rev. Lett.* **88** 127001
[7] Fogg A M, Meldrum J, Darling G R, Claridge J B and Rosseinsky M J 2006 *J. Am. Chem. Soc.* **128** 10043
[8] Bharathi A, Balaselvi S J, Premila M, Sairam T N, Reddy G L N, Sundar C S and Hariharan Y 2002 *Solid State Commun.* **124** 423
[9] Souptela D, Hossainb Z, Behra G, Lösera W and Geibel C 2003 *Solid State Commun.* **125** 17
[10] Fogg A M, Chalker P R, Claridge J B, Darling G R and Rosseinsky M J 2003 *Phys. Rev. B* **67** 245106
[11] Fogg A M, Claridge J B, Darling G R and Rosseinsky M J 2003 *Chem. Commun.* **12** 1348
[12] Gao M, Lu Z Y and Xiang T 2015 *Phys. Rev. B* **91** 045132
[13] Bazhirov T, Sakai Y, Saito S and Cohen M L 2014 *Phys. Rev. B* **89** 045136
[14] Gao M, Yan X W, Lu Z Y and Xiang T 2020 *Phys. Rev. B* **101** 094501
[15] Haque E, Hossain M A and Stampfl C 2019 *Phys. Chem. Chem Phys.* **21** 8767
[16] Zhu L, Borstad G M, Liu H, Guńka P A, Guerette M, Dolyniuk J A, Meng Y, Greenberg E, Prakapenka V B, Chaloux B L, Epshteyn A, Cohen R E and Strobel T A 2020 *Sci. Adv.* **6** 8361
[17] Giannozzi P, Baroni S, Bonini N, *et al.* 2020 *J. Phys.: Condens. Matter* **21** 395502
[18] Giustino F, Cohen M L and Louie S G 2007 *Phys. Rev. B* **76** 165108
[19] Perdew J P, Burke K and Ernzerhof M 1996 *Phys. Rev. Lett.* **77** 3865
[20] Hamann D R 2013 *Phys. Rev. B* **88** 085117
[21] Methfessel M and Paxton A T 1989 *Phys. Rev. B* **40** 3616
[22] Baroni S, De Gironcoli S, Dal Corso A and Giannozzi P 2001 *Rev. Mod. Phys.* **73** 515
[23] Pizzi G, Vitale V, Arita R, *et al.* 2020 *J. Phys.: Condens. Matter* **32** 165902
[24] Poncé S, Margine E R, Verdi C and Giustino F 2016 *Comp. Phys. Commun.* **209** 116
[25] Choi H J, Cohen M L and Louie S G 2003 *Physica C* **385** 66
[26] Margine E R and Giustino F 2013 *Phys. Rev. B* **87** 024505
[27] Lazicki A, Yoo C S, Cynn H, Evans W J, Pickett W E, Olamit J, Liu K and Ohishi Y 2007 *Phys. Rev. B* **75** 054507
[28] Buzea C and Yamashita T 2001 *Supercond. Sci. Technol.* **14** 115
[29] Eiguren A and Ambrosch-Draxl C 2008 *Phys. Rev. B* **78** 045124

[30] Calandra M, Profeta G and Mauri F 2010 *Phys. Rev. B* **82** 165111
[31] Richardson C F and Ashcroft N W 1997 *Phys. Rev. Lett.* **78** 118
[32] Lee K H, Chang K J and Cohen M L 1995 *Phys. Rev. B* **52** 1425
[33] Allen P B and Dynes R C 1975 *Phys. Rev. B* **12** 905
[34] Monteverde M, Nu Núñez-Regueiro M, Rogado N, Regan K A, Hayward M A, He T, Loureiro S M and Cava R J 2001 *Science* **292** 75
[35] Lorenz B, Meng R L and Chu C W 2001 *Phys. Rev. B* **64** 012507
[36] Tomita T, Hamlin J J, Schilling J S, Hinks D G and Jorgensen J D 2001 *Phys. Rev. B* **64** 092505
[37] Saito E, Taknenobu T, Ito T, Iwasa Y, Prassides K and Arima T 2001 *J. Phys.: Condens. Matter* **13** L267
[38] Deemyad S, Schilling J S, Jorgensen J D and Hinks D G 2001 *Physica C* **361** 227
[39] Loa I and Syassen K 2001 *Solid State Commun.* **118** 279
[40] Pogrebnyakov A V, Redwing J M, Raghavan S, Vaithyanathan V Schlom D G, Xu S Y, Li Q, Tenne D A, Soukiassian A, Xi X X, Johannes M D, Kasinathan D, Pickett W E, Wu J S and Spence J C H 2004 *Phys. Rev. Lett.* **93** 147006
[41] Gubser D U and Webb A W 1975 *Phys. Rev. Lett.* **35** 104
[42] Thomasson J, Ayache C, Spain I L and Villedieu M 1990 *J. Appl. Phys.* **68** 5933
[43] Hamlin J J, Tissen V G and Schilling J S 2006 *Phys. Rev. B* **73** 094522
[44] Yabuuchi T, Matsuoka T, Nakamoto Y and Shimizu K 2006 *J. Phys. Soc. Jpn.* **75** 083703
[45] Balster H and Wittig J 1975 *J. Low Temp. Phys.* **21** 377
[46] Porsch F and Holzapfel W B 1993 *Phys. Rev. Lett.* **70** 4087
[47] Tissen V G, Ponyatovskii E G, Nefedova M V, Porsch F and Holzapfel W B 1996 *Phys. Rev. B* **53** 8238
[48] Schilling J S 2007 *Physica C* **182** 460
[49] Chen W, Semenok D V, Troyan I A, Ivanova A G, Huang X, Oganov A R and Cui T 2020 *Phys. Rev. B* **102** 134510
[50] Wan X, Dong J, Weng H and Xing D Y 2001 *Phys. Rev. B* **65** 012502